Science Bulletin 64 (2019) 934–940

Contents lists available at ScienceDirect

Science Bulletin

journal homepage: www.elsevier.com/locate/scib

Article

Hierarchically spacing DNA probes on bio-based nanocrystal for spatial detection requirements

Lin Gan [a,b,1], Ya Wang [a,b,1], Meng Zhang [a,b], Xuehuan Xia [a,b], Jin Huang [a,b,*]

[a] Key Laboratory of Luminescence and Real-Time Analytical Chemistry, Ministry of Education, School of Chemistry and Chemical Engineering, Southwest University, Chongqing 400715, China
[b] Chongqing Key Laboratory of Soft-Matter Material Chemistry and Function Manufacturing, Southwest University, Chongqing 400715, China

ARTICLE INFO

Article history:
Received 22 April 2019
Received in revised form 9 May 2019
Accepted 14 May 2019
Available online 18 May 2019

Keywords:
Cellulose nanocrystal
DNA fluorescence probe
Steric spacing
Surface modification
Mercury ion detection

ABSTRACT

Sterically spacing and locating functional matters at the nanoscale exert critical effects on their application, especially for the fluorescence probes whose aggregation causes emission quenching. Here we achieved a hierarchical spacing strategy of DNA fluorescence probes for ion detection via locating them separately on rod-like cellulose nanocrystals (CNCs) and further isolating CNCs by pre-grafting long molecular chains. Controlling chemical structure of CNC and location degree could adjust the interspace of DNA probes (with a molecular length of ca. 3.6 nm) in a range of 3.5–6.5 nm with a gradient about 0.2 nm. A length up to micrometer scale of the CNC nanorods was necessary to provide DNA probes with well-separated grafting locations and enough freedom, which brought a vast linear detection range from 10 nmol/L to 5 μmol/L of Hg^{2+} concentration. The abundant reactive sites on CNC allowed a grafting pre-location of poly (tert-butyl acrylate) (P*t*BA) to promote the isolation of DNA probes. Controlled radical polymerization was employed to adjust the length of P*t*BA molecular chains, which increased the linear sensitivity coefficient of Hg^{2+} detection by ca. 2.5 times. This hierarchical nanoscale spacing concept based on chemical design can hopefully conduce to the development of biosensor and medical diagnosis. A hierarchical spacing strategy was applied to separate DNA fluorescent probes on CNCs and detect ion concentration linearly. The first-level spacing was to locate probes uniformly on CNCs, obtaining a wide linear range; and the second-level spacing was to isolate CNCs with polymer, obtaining an increased linear coefficient.

1. Introduction

Regular spacing of nanomaterials or nanoscale-controlled spacing of matters brings various functional benefits [1–4], whereas their high specific areas usually cause an uncontrollable aggregation. In the detection technology based on fluorescence probes, the detection sensitivity decreased sensitively as the probes aggregate [5–8]. Especially for the DNA fluorescence probes, the long and flexible chains of DNA molecules increase the difficulty in spacing the probes.

For sterically spacing and locating the fluorescence probes on DNA molecules, the DNA has been designed and assembled with a two-dimensional (2D) or three-dimensional (3D) structure [9–16]. Fan and his co-workers [12,16] have prepared an Hg^{2+}-responsive DNA tetrahedral with one edge containing the rich-thymine (rich-T) sequence, which decreased the detection limit to 20 nmol/L. Those fluorescent probes enjoy a lower cost and higher portability for fast real-time detection, compared to other method on Hg^{2+} detection, such as inductively coupled plasma mass spectrometry (ICP-MS), atomic absorption/emission spectroscopy [17,18], anodic stripping voltammetry [19], and capillary electrophoresis [20].

However, such 2D or 3D DNA structures required long base sequence and leaded to a high cost and long preparing time. Grafting the DNA fluorescence probes on templates is another way to space the probes [21–26]. Ting and his co-workers [27] prepared rich-thymine (rich T) DNA-derived bio-dots with a mercury (II) (Hg^{2+}) detection linear range of 0–0.5 μmol/L, which used the dots to space DNA and emit concurrently. Gold nanoparticles [28], silver nanoclusters [29], carbon nanotube [26] mesoporous silica [30], and metal–organic framework [31] were also used as templates of DNA fluorescence sensor to detect Hg^{2+} concentration. Unfortunately, the templates just spaced the probes on a single template, the aggregation of templates could still cause the contact of probes.

* Corresponding author.
E-mail address: huangjin2015@swu.edu.cn (J. Huang).
[1] These authors contributed equally to this work.

https://doi.org/10.1016/j.scib.2019.05.013
2095-9273/

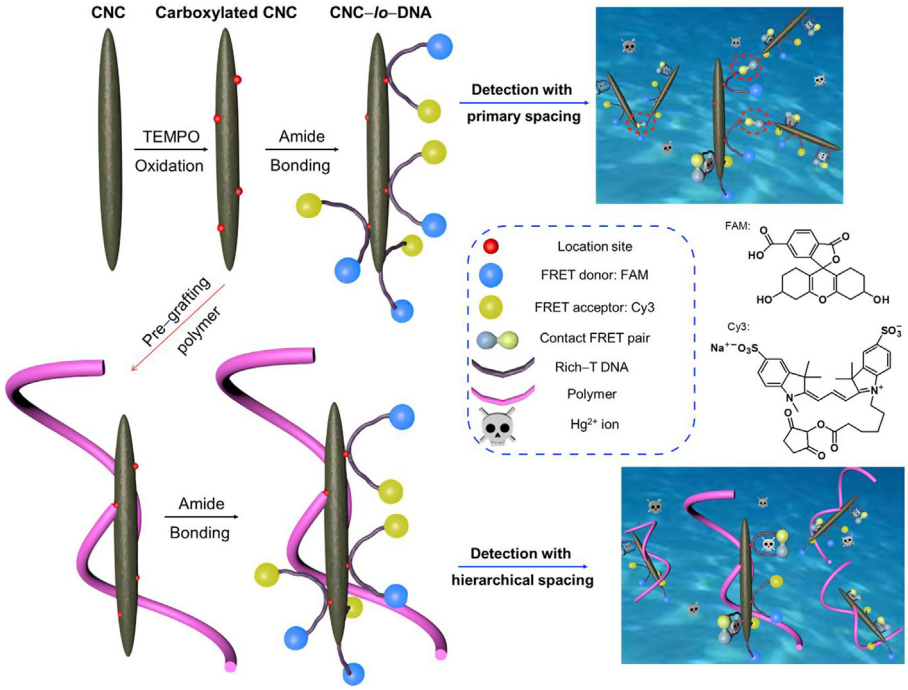

Scheme 1. Hierarchical spacing strategy to separate rich-T DNA fluorescence probes and increase Hg^{2+} detection sensitivity. Uniformly separated grafting location sites were set on CNC via TEMPO-mediated oxidation carboxylation, and DNA probes were primarily spaced via a degree-controllable chemical location on CNC. The primary spacing could not avoid the contact between CNC nanoparticles, which cause non-Hg^{2+}-induced FRET (red break cycle in the left down image). Pre-grafting polymers on CNC could avoid the contact and further isolate the probes on different CNC nanoparticles (right down image), increasing the detection sensitivity.

To increase the sensitivity of DNA fluorescence probes on templates further, a hierarchical spacing strategy is still needed to control the steric space between the probes. Herein, we first separately located the rich-T DNA fluorescence probes on rod-like cellulose nanocrystals (CNCs) by using the long inter-distance of location sites on CNCs, as shown in Scheme 1. The abundant grafting sites also allowed us to pre-graft polymer chains to isolate the probes secondary. We also studied the effects of the length and chemical structure of CNC on spacing DNA fluorescence probes and their sensitivity for detecting Hg^{2+}.

2. Materials and methods

2.1. Materials

The cotton was purchased from Hubei Chemical Fiber Group Co., Ltd. (China). The sodium hypochlorite solution with 6wt%–14wt% active chlorite, 1-Ethyl-3-(3-dimethylaminopropyl) carbodiimide hydrochloride (EDC), trimethylamine, dimethyl formamide (DMF), dichloromethane, 2-bromoisobutyryl bromide, *N*,*N*,*N*′,*N*′,*N*″-pentamethyldiethylenetriamine (PMDETA), *tert*-butyl acrylate (*t*BA), and *N*-hydroxysuccinimide (NHS) was purchased from Sigma-Aldrich Inc. (St. Louis, MO). The 2,2,6,6-tetramethylpiperidine-1-oxyl (TEMPO, 98%), 2-morpholinoethanesulfonic acid monohydrate (MES), solution of 33wt% hydrogen chloride (HCl), sodium hydroxide (NaOH), ethanol, acetic acid, tetrahydrofuran (THF), and sodium bromide (NaBr) were purchased from Macklin Chemical Inc. (Shanghai, China). The dialysis tubing (Float-A-Lyzer MWCO 10000) and Mikrocross ultrafilters were purchased from Spectrum Laboratories Inc. (Rancho Dominguez, CA). Hg^{2+} stock solution (0.1 mol/L) was prepared by dissolving $Hg(NO_3)_2$ with 0.5wt% HNO_3. The pH of the Hg^{2+} stock solution was adjusted to 6.0, to prevent the formation of HgO particles. Milli-Q water (18.2 MΩ/cm) was used for all experiments.

The 6-FAM and Cy3 dual-labelled DNAs were synthesized and purified by Sangon Biotech Shanghai Co. Ltd. (Shanghai, China). The sequence of the oligonucleotide-involved DNA was as followed: 5-(6-FAM)-CTT GTT GTC CT (-amino C12) G TTG TTG TTC-Cy3-3 (Mercury-specific oligonucleotide). A 0.1 mol/L sodium phosphate buffer (pH 7.2) containing 0.1 mol/L NaCl was used as the working buffer. The length of the DNA probe was calculated according to the length of nucleobases [32].

2.2. CNC preparation and surface modification

The cCNC was prepared from pure cotton cellulose by sulfuric acid hydrolysis [33]. Briefly, 25 g cotton was immersed into a 1 L 2wt% NaOH solutions for 12 h with mechanical stirring, and 12.5 g obtained fibers were immersed in a 250 mL aqueous solution of 65wt% H_2SO_4 at 45 °C for 60 min with mechanical stirring. The obtained suspension was centrifuged and washed with distilled water until its pH > 6, and then dialyzed against deionized water for five days. After that, the suspension was concentrated and then dispersed into deionized water to obtain cCNC dispersion by ultrasonic treatment for 15 min using a Branson sonifier equipped with a microtip and power setting of 4.

The tCNC was obtained from tunicate cellulose as followed [34]. 10 g tunicate powders pretreated with 200 mesh sieve were dispersed in a 300 mL aqueous solution of 5 wt% KOH with mechanic stirring. After a 12 h reaction at 80 °C, the solid product was centrifuged out and washed by water until pH ~ 7. The obtained powders reacted twice with 10 mL acetic acid and a 7.1 mL 4wt%–6wt% aqueous solution of NaClO at 60 °C. After centrifugation, washing until pH ~ 7, and drying at 60 °C, the obtained powders (4 g) were dispersed into 400 mL water with a 120 s low-speed treatment and 240 s high-speed treatment of a waring blender (HGB2WTS3, Waring commercial). 270 mL 65wt% aqueous solution of H_2SO_4 was added into the dispersion. After a 4 h reaction at 50 °C under stirring, the product was centrifuged out and washed by water until

pH ~ 7. After a dialysis with deionized water for 7 days, the tCNC dispersion was obtained. The tCNC powders were then obtained by freeze-drying.

2.3. Carboxylating CNC

The obtained CNC dispersion, for both cCNC and tCNC, was treated via TEMPO-mediated carboxylation to convert the surface 6-site primary hydroxyls of cellulose to COOH groups [35–37]. Briefly, a 100 mL aqueous solution of 1.88 mmol/L TEMPO and 31.4 mmol/L NaBr was added into a 100 mL 0.01wt% CNC dispersion within 20 min under mechanically stirring. The carboxylation started when 10 mL 7.5wt% NaClO solution was added into the dispersion. The pH was adjusted to 10 at room temperature by adding a 10 mL aqueous solution of 0.5 mol/L NaOH. After a certain time of stirring, the reaction was terminated with ethanol (ca. 4 mL) and the pH was adjusted to 7 with 0.5 mol/L HCl. The suspension was centrifuged and washed with deionized water five times. The obtained carboxylated cCNC (OcCN) and carboxylated tCNC (OtCN) were dialyzed against deionized water and then stored at 4 °C.

2.4. Locating DNA probes on CNCs

Locating the amino-modified DNA onto the CNC, for both cCNC and tCNC, was performed via a carboxylation-amidation reaction [38]. This reaction created a covalent amide bond between the primarily amino-modified ssDNA and carboxylated CNC by COOH–NH_2 coupling. Briefly, a 200 μL 0.1wt% carboxylated CNC suspension was added into a mixing solution of EDC (1 mg/mL) and NHS (1 mg/mL) at 4 °C under stirring. The pH was kept at ca. 5.7 with a buffer of 0.05 mol/L MES/0.5 mol/L NaCl. After a reaction of 30 min, the excess reactants were removed from the EDC-activated carboxylated CNC by alternately concentrating with a MicroKross ultrafilter (MWCO 50 kD) and diluting with filtered deionized water. The obtained EDC-activated carboxylated CNC was added into a certain-volume solution of 0.65 μmol/L amino-modified DNA oligomer in 1 mmol/L phosphate buffer (pH ~ 7.2) with 0.5 mol/L NaCl. After 12 h, the product, cCNC-*lo*-DNA (or tCNC-*lo*-DNA), was centrifuged out and washed by deionized water five times, and then stored in a 1 mmol/L phosphate buffer (pH ~ 7.2) at –20 °C.

2.5. Pre-grafting polymer on CNC-lo-DNA

1 g tCNC was dispersed in 33 mL triethylamine and 100 mL DMF under nitrogen protection [39]. 26 mL 2-bromoisobutyryl bromide was added dropwise into the dispersion. After a 24 h reaction at 70 °C, the solid product was centrifuged out. The solid was then treated by a 24 h Soxhiet extraction with dichloromethane and ethanol to obtained Br-grafted tCNC. 0.6 g Br-grafted tCNC was dispersed into a 4.86 mL DMF solution of 23.7 mmol/L CuBr, 47.3 mmol/L PMDETA, 11.7 mmol/L EBiB, and a certain concentration of tBA. After a 12 h reaction at 75 °C under nitrogen protection, the tCNC pre-grafting poly (*tert*-butyl acrylate) (P*t*BA) was obtained by centrifugation and washing with water. The obtained product was grafted by DNA probes with the method of "Carbodiimide coupling of oligonucleotide and CNCs", and coded as tCNC-*lo*-DNA/P*t*BA.

2.6. COOH content measurement

A 50 mg sample was dispersed into a 15 mL aqueous solution of 0.01 mol/L HCl with stirring and then titrated by a solution of 0.01 mol/L NaOH [40]. The COOH content was obtained with the curve of electric conductivity titration and Eq. (1):

$$\text{COOH content} = \frac{c_{\text{NaOH}}(V_2 - V_1)}{m_s}, \quad (1)$$

where c_{NaOH} and m_s are the concentration of NaOH solution and the mass of sample, respectively. Fig. S1 (online) shows the method to obtained V_2 and V_1.

2.7. FRET measurement

Fluorescence measurements were carried out with an F-7000 Fluorescence spectrophotometer (Hitachi, Japan). A PBS buffer of 1 mmol/L (pH 7.2) was used as the working buffer. The stock solutions were prepared in PBS buffer and stored at −20 °C. The aqueous Hg^{2+} solutions were prepared with 0.5% HNO_3 to avoid hydrolyzation. One volume of 5 μL of the above Hg^{2+} solution was introduced into a 2 mL CNC-*lo*-DNA dispersion with a concentration of 5 nmol/L. After incubation for 20 min at room temperature, the spectra of FAM and Cy3 in the probe were recorded with excitation wavelength of 492 nm. The ratio of the fluorescence intensity at the emission wavelength 564 and 518 nm ($r_{564/518}$) was used as the semi-quantitative value of the FRET effect. The linear coefficient was the slope of the OLS (ordinary least square) fitting curve of the relationship between $r_{564/518}$ and Hg^{2+} concentration. The beginning of the linear range for Hg^{2+} detection was set as 3σ/(linear slope), where σ is the standard deviation of the background change [41]. The end of the linear range was the Hg^{2+} concentration whose $r_{564/518}$ was *s*% higher or lower than the fitting curve, where *s*% was the standard deviation of the fitting.

2.8. Instruments

2.8.1. Microscope measurements

The Atom force microscope (AFM) images were obtained with a Dimension ICON AFM (Digital Instruments, Bruker) at a tapping mode of a 3.0 V amplitude with samples on mica plates and analyzed by a software of Gwyddion 2.19. Transmission electron microscope (TEM) images were obtained with a JEOL JEM-1200EX TEM (Tokyo, Japan) at an accelerating voltage of 100 kV.

2.8.2. Zeta potential measurement

The zeta-potential was measured with a Zetasizer Nano ZS90 (Malvern Instruments Ltd., Worcestershire, United Kingdom).

2.8.3. Gel permeation chromatogram (GPC)

The GPC measurement was conducted with a Waters Chromatography (model 1515–2414) equipped by a DRI detector of type 410, a two-angle light-scattering detector of type PD2040, and a 7.5 mm B-300 chromatographic column of type tricolumn-series-polymer (Laboratories PLgel 10 μm). The test was conducted at 35 °C with absolute THF as the eluent (speed: 1.00 mL/min) and polystyrene ($M_p = 9 \times 10^4$ g/mol, $M_w/M_n < 1.04$) as the calibration polymer.

3. Results

3.1. First-level space DNA probes located on CNC

Two CNCs with different lengths were chosen to graft DNA probes: one extracted from cotton (cCNC, ca. 140 nm) and another extracted from tunicate (tCNC, ca. 2 μm) (as shown in Fig. S2 online). Fig. 1 shows the FT-IR spectra of the nanoparticles in the different steps to locate probes onto CNC. Insets of Fig. 1a and b show that only the final location products, cCNC-*lo*-DNA and tCNC-*lo*-DNA, owned an FT-IR peak of –NH at 1,548 cm^{-1}, which came from the DNA molecules. Those results indicated that the DNA probes were located on cCNC and tCNC with amide bonds

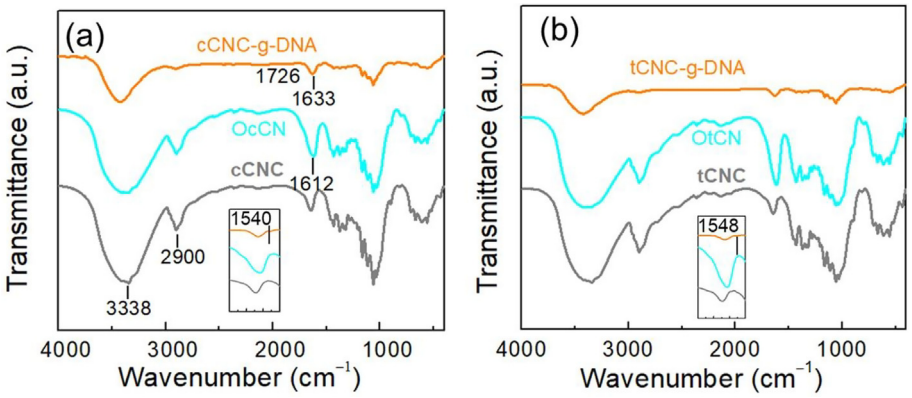

Fig. 1. The FT-IR spectra (a) cCNC, OcCN, and cCNC-*lo*-DNA; and (b) tCNC, OtCN, and tCNC-*lo*-DNA. OcCN and OtCN refer to the TEMPO-mediated carboxylated cCNC and tCNC, respectively. The (a inset) and (b inset) are the FTIR spectra in a range from 1,800 to 1,500 cm^{-1}. The COOH contents in both OcCN and OtCN were 0.3 mmol/g. Both the cCNC-*lo*-DNA and tCNC-*lo*-DNA were obtained with a 1:1 molar regent ratio between COOH on carboxylated CNC and DNA (MRT C/D).

[42]. The TEM and AFM images also indicated that the shape and size of cCNC and tCNC changed little after locating DNA probes, as shown in Fig. S2 (online), which meant the location did not induce the CNC aggregation.

Adjusting the location degree (D_l) of DNA probes on CNC was based on controlling the COOH content on carboxylated CNC. With different carboxylating reaction time, the COOH contents on OcCN and OtCN were adjusted from 0.04 to 0.30 mmol/g and from 0.11 to 0.30 mmol/g, respectively, as shown in Fig. 2a. The D_l of DNA probes on CNC then varied with different molar regent ratios between DNA and the COOH on carboxylated CNC, as shown in Fig. 2b and c [43]. We further calculated the average space between DNA probes (inter-space) on CNC (Fig. 2d and e) with Eq. (2):

$$d_{in} = \sqrt{\frac{4}{D_l N_A \rho d}}, \tag{2}$$

where d_{in} is the inter-distance, D_l is measured and calculated with Eq. (3), N_A is the Avogadro number, ρ is the density of CNC (1.6 g/cm^3), and d is the average diameter of CNC (10–20 nm).

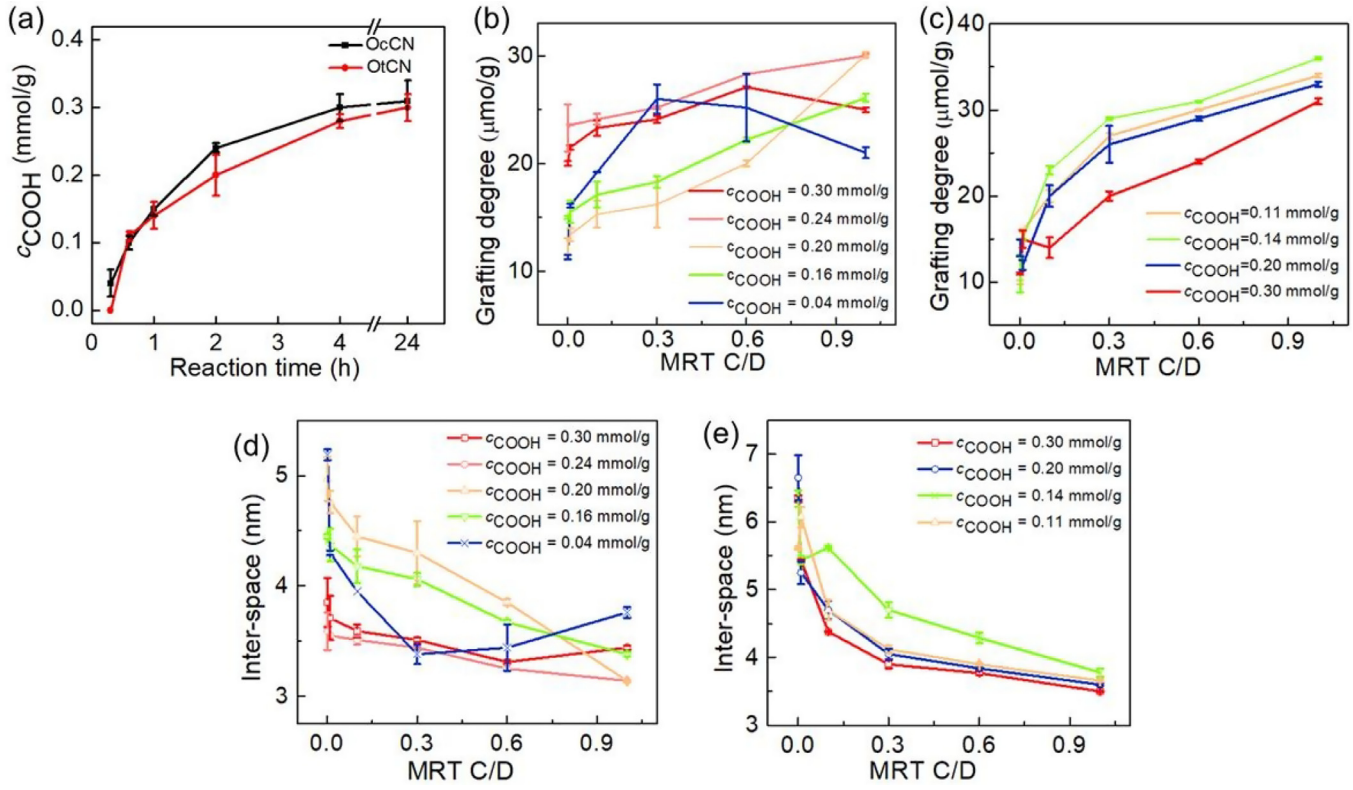

Fig. 2. The controlled inter-space between DNA fluorescence probes on CNC by adjusting preparing methods. (a) The relationship between the TEMPO-mediated carboxylating reaction time and the COOH content on OcCN and OtCN. The relationships (b) between the location degree (D_l) of DNA probes on cCNC and MRT C/D, (c) between the D_l of DNA probes on tCNC and MRT C/D, (d) between inter-space of DNA probes on cCNC and MRT C/D, and (e) between inter-space of DNA probes on tCNC and MRT C/D.

$$D_1 = c_{CC} - c_{FP,} \quad (3)$$

where c_{CC} and c_{FP} refer to the COOH contents on carboxylated CNC and final products of probe grafting.

The results indicated that the DNA probes were spaced in the first level with an inter-space covering a range from 3.1 to 5.1 nm in an accuracy of 0.1 nm on cCNC and from 3.5 to 6.5 nm in an accuracy of 0.2 nm on tCNC, respectively.

Hg^{2+} with different concentration could induce the varied degree of fluorescent resonance energy transferring (FRET) between the FAM and Cy3 in the rich-T DNA of this work, as shown in Fig. 3a. The Fig. 3a inset also shows that photoluminescence (PL) spectra of DNA probes (not on CNC) at different Hg^{2+} concentration presented a lower FRET effect than those on CNC. However, the linear range of the relationship between the FRET effect and Hg^{2+} concentration was much less stable for cCNC-*lo*-DNA than that for tCNC-*lo*-DNA, as shown in Fig. 3b and c. Since the inter-space control gradient on cCNC was twice more accurate than that on tCNC, the high stability of tCNC should be related to its longer length. The long length of tCNC (14.3 times of cCNC) may provide DNA probes more space to locate uniformly on tCNC, which leading to a more stable FRET effect. The evolution of the linear coefficient for detecting Hg^{2+} concentration at different COOH content and inter-space was also more regular with tCNC than cCNC, as shown in Fig. 3d and e.

3.2. Second-level spacing DNA probes

Although the FRET linear range of tCNC-*lo*-DNA was more stable and wider than that of cCNC-*lo*-DNA, the average linear coefficient of tCNC-*lo*-DNA (0.7207 L/nmol) was just about one third of that of cCNC-*lo*-DNA (2.1494 L/nmol). The lower coefficient might come from the fact that longer particles contact easilier in their dispersion, which could cause the connection of DNA probes on different tCNC nanoparticles. The similar electrostatic repulsions of cCNC-*lo*-DNA nanoparticles (ζ-potential = −48 mV) and tCNC-*lo*-DNA nanoparticles (ζ-potential = −52 mV) also suggested that here the length rather than the surface charge strongly affected the coefficient. We thus pre-grafted a polymer, P*t*BA, on tCNC-*lo*-DNA to space the DNA probes on different tCNC nanoparticles in the second level.

Fig. 4a shows the typical FT-IR spectrum of P*t*BA-grafting products (tCNC-*lo*-DNA/P*t*BA). The sharp peak of carbonyl at 1,725 cm^{-1}, which tCNC-*lo*-DNA did not owned, proved that the PtBA was grafted onto the tCNC-*lo*-DNA with ester bonds. The characteristic peak of the tertiary alkyl from P*t*BA at 1,370 cm^{-1} was also observed. The molar mass of P*t*BA was adjusted by tuning the molar reagent between *t*BA and initiator EBiB (n_{tBA}:n_{EBiB}), as shown in Fig. 4b. Fig. 4c and d indicate that the FRET linear coefficient was stable and kept in a range from 10 nmol/L to 5 μmol/L with P*t*BA of different molar masses. Fig. 4d shows that the linear Hg^{2+}-detection coefficient of DNA probes on tCNC increased by ca. 2.5 times after grafting a P*t*BA of 4.8×10^3 g/mol (total length ≃47.2 nm) shows the relationship between the $I_{564\ nm}/I_{519\ nm}$ of the tCNC-*lo*-DNA/P*t*BA and the Hg^{2+} concentration with different molar masses of P*t*BA. When the molecular mass of P*t*BA increased from 0 to 4.8×10^3 g/mol, the P*t*BA could separate the different CNC nanoparticles in an increasing degree, leading to a more sensitive fluorescent detection with DNA probes on CNC. However, further increasing the molar masses of P*t*BA severely reduced the ζ-potential of the nanoparticles, as shown in Fig. 4e. This feature may promote the contact between the nanoparticles and then decrease the coefficient, as shown in Fig. 4d.

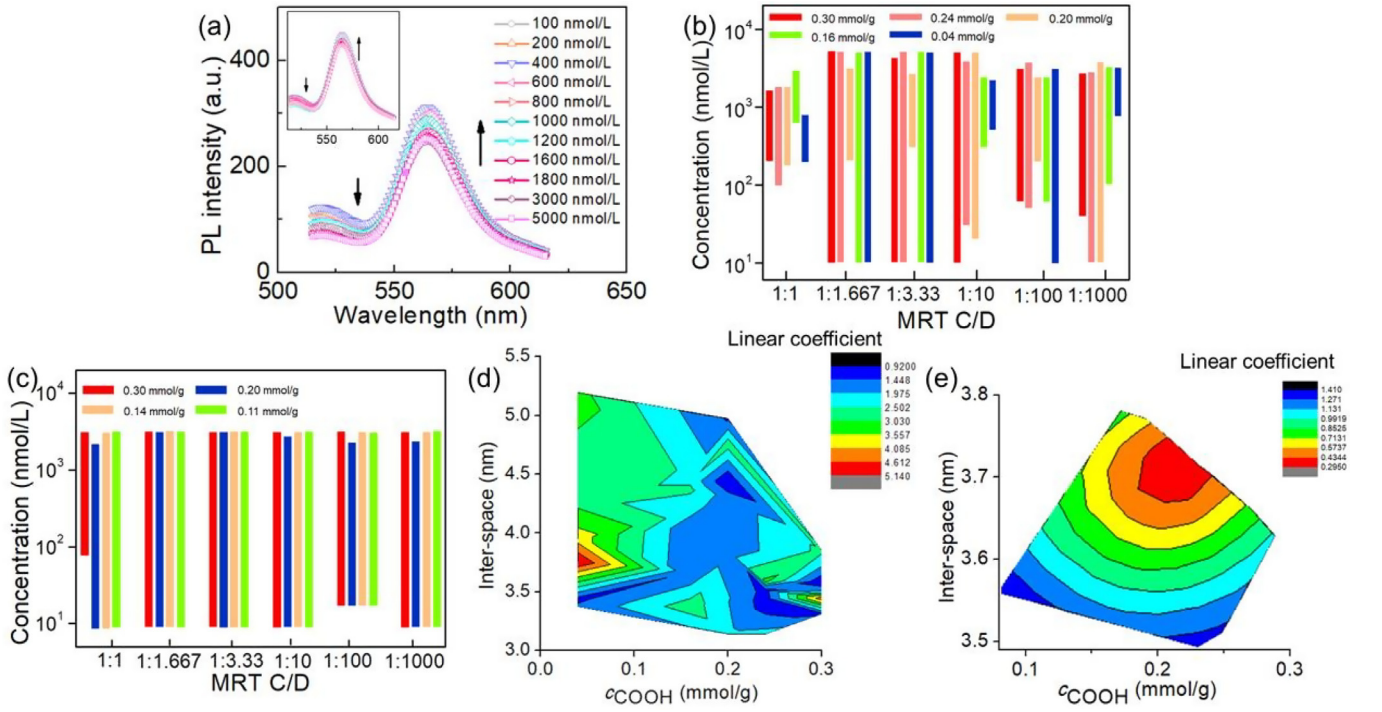

Fig. 3. The linearity of Hg^{2+} concentration detection with DNA fluorescence probes on CNC. (a) PL spectra of cCNC-*lo*-DNA prepared with an OcCN containing 0.30 mmol/g COOH and MRT C/D of 1:1 at different Hg^{2+} concentration. (a) inset is the PL spectra of DNA probes (not on CNC) at different Hg^{2+} concentration. The linear range to detect Hg^{2+} with (b) cCNC-*lo*-DNA and (c) tCNC-*lo*-DNA fluorescence probes prepared at different MRT C/D with carboxylated CNCs owning different COOH contents. The linear coefficient to detect Hg^{2+} with (d) cCNC-*lo*-DNA and (e) tCNC-*lo*-DNA fluorescence probes at different inter-spacing and prepared with carboxylated CNCs owning different COOH contents.

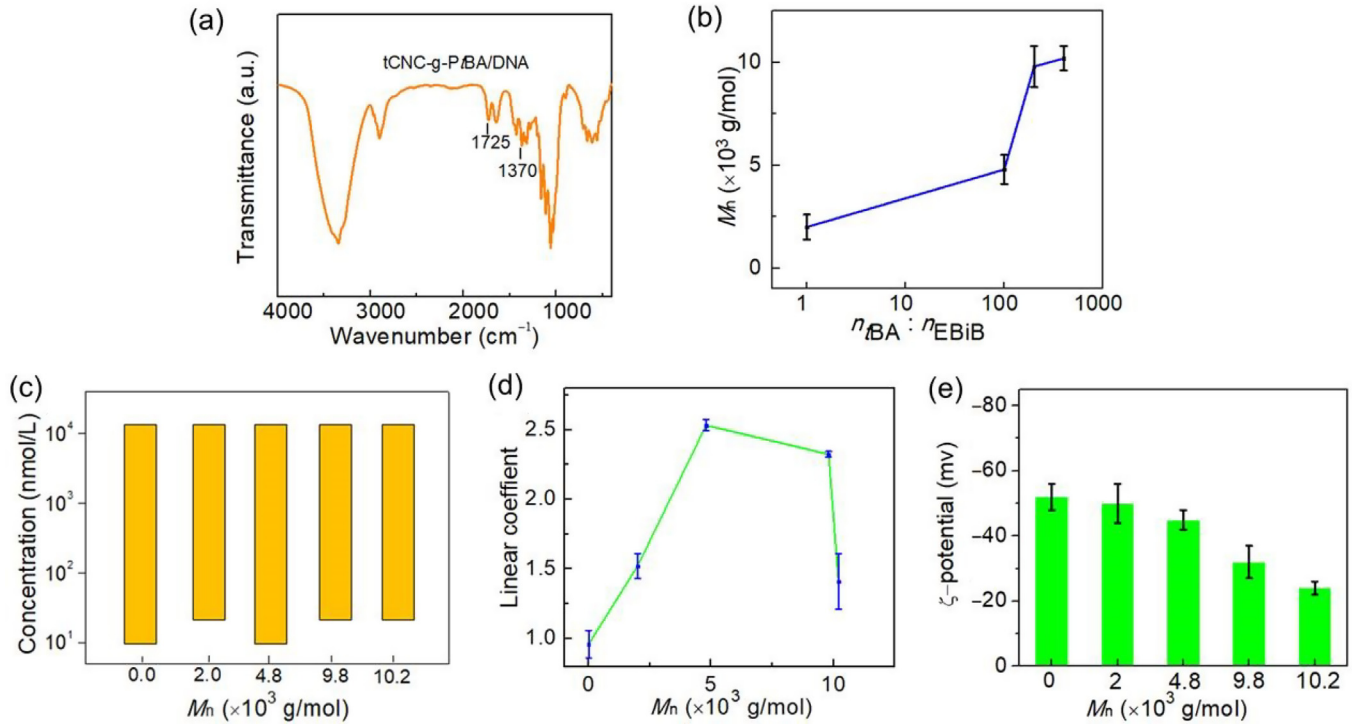

Fig. 4. The effect of pre-grafting polymers on the linearity of Hg^{2+} concentration detection with DNA fluorescence probes on tCNC. (a) FT-IR spectrum of CNC-*lo*-DNA/P*t*BA. (b) Relationship between molecular mass of P*t*BA and molecular ratio of monomer *t*BA and initiator EBiB. (c) Linear ranges, (d) linear coefficient, and (e) ζ-potential (detecting Hg^{2+}) of tCNC-*lo*-DNA/P*t*BA fluorescence probes prepared by OtCN containing 0.20 mmol/g COOH content with MRT C/D of 1:3.33 and different molar masses of P*t*BA.

4. Conclusions and implication

Summarily, at the first level of spacing matters on a single CNC nanorod, DNA probes were separated with an inter-space of 3.5–6.5 nm in an 0.2 nm accuracy by controlling the carboxyl functionality on CNC and location degree of DNA on CNC. The higher aspect-ratio CNC with a length of ca. 2 μm provided probes with enough space to locate on CNC uniformly and obtain a stable and wide linear range (from 10 nmol/L to 5 μmol/L) of detecting Hg^{2+}. At the second spacing level of isolating the DNA probes on different CNC nanorods, P*t*BA was pre-grafted on CNC and controlled to be a proper chain length of ca. 47.2 nm leading to a ca. 2.5 times increase in linear coefficient. Overall, the hierarchical spacing of DNA probes has been achieved via the concept of "molecular engineering on programmed nanocrystal surface", which not only offered a new design of highly sensitive detection, but opened a method to chemically operate matter in space at nanoscale for more advanced applications.

Conflict of interest

The authors declare that they have no conflict of interest.

Acknowledgments

This research was financially supported by the National Natural Science Foundation of China (51603171 and 51373131), Talent Project of Southwest University (SWU115034), Fundamental Research Funds for the Central Universities (XDJK2016C032), Key Laboratory of Polymeric Composite & Functional Materials of Ministry of Education (PCFM201605) and Hubei Key Laboratory of Advanced Textile Materials & Application (Fzxcl2017003).

Author contributions

Jin Huang conceived the idea of this study and conducted the experiment; Lin Gan improved the experimental design and detailedly analyzed results; Ya Wang carried out experiments and analyzed results; Xuehuan Xia and Meng Zhang assisted with testing. All authors discussed the results and revised the manuscript.

Appendix A. Supplementary data

Supplementary data to this article can be found online at https://doi.org/10.1016/j.scib.2019.05.013.

References

[1] Srinivasan K, Subramanian K, Murugan K, et al. Fluorescence quenching of MoS_2 nanosheets/DNA/silicon dot nanoassembly: effective and rapid detection of Hg^{2+} ions in aqueous solution. Environ Sci Pollut Res 2018;25:10567–76.
[2] Shi Y, Chen N, Su Y, et al. Silicon nanohybrid-based SERS chips armed with an internal standard for broad-range, sensitive and reproducible simultaneous quantification of lead (II) and mercury (II) in real systems. Nanoscale 2018;10:4010–8.
[3] Qu X, Yang F, Chen H, et al. Bubble-mediated ultrasensitive multiplex detection of metal ions in three-dimensional DNA nanostructure-encoded microchannels. ACS Appl Mater Inter 2017;9:16026–34.
[4] Gan L, Liao J, Lin N, et al. Focus on gradientwise control of the surface acetylation of cellulose nanocrystals to optimize mechanical reinforcement for hydrophobic polyester-based nanocomposites. ACS Omega 2017;2:4725–36.
[5] Li D, Wieckowska A, Willner I. Optical analysis of Hg^{2+} ions by oligonucleotide-gold-nanoparticle hybrids and DNA-based machines. Angew Chem Int Ed 2008;47:3927–31.
[6] Tanaka Y, Kondo J, Sychrovský V, et al. Structures, physicochemical properties, and applications of T-Hg II-T, C-Ag I-C, and other metallo-base-pairs. Chem Commun 2015;51:17343–60.
[7] Zhu S, Zhuo Y, Miao H, et al. Detection of mercury (II) by DNA templated gold nanoclusters based on forming thymidine-Hg^{2+}-thymidine duplexes. Luminescence 2015;30:631–6.

[8] Liu Y, Dong X, Chen P. Biological and chemical sensors based on graphene materials. Chem Soc Rev 2012;41:2283–307.
[9] Goodman RP, Heilemann M, Doose S, et al. Reconfigurable, braced, three-dimensional DNA nanostructures. Nat Nanotechnol 2008;3:93–6.
[10] Zhang F, Jiang S, Wu S, et al. Complex wireframe DNA origami nanostructures with multi-arm junction vertices. Nat Nanotechnol 2015;10:779–84.
[11] Lu N, Pei H, Ge Z, et al. Charge transport within a three-dimensional DNA nanostructure framework. J Am Chem Soc 2012;134:13148–51.
[12] Pei H, Lu N, Wen Y, et al. A DNA nanostructure-based biomolecular probe carrier platform for electrochemical biosensing. Adv Mater 2010;22:4754–8.
[13] Song P, Li M, Shen J, et al. Dynamic modulation of DNA hybridization using allosteric DNA tetrahedral nanostructures. Anal Chem 2016;88:8043–9.
[14] Jones MR, Seeman NC, Mirkin CA. Programmable materials and the nature of the DNA bond. Science 2015;347:1260901–11.
[15] Han D, Pal S, Yang Y, et al. DNA gridiron nanostructures based on four-arm junctions. Science 2013;339:1412–5.
[16] Pei H, Liang L, Yao G, et al. Reconfigurable three-dimensional DNA nanostructures for the construction of intracellular logic sensors. Angew Chem Int Ed 2012;51:9020–4.
[17] Gómez-Ariza JL, Lorenzo F, García-Barrera T. Comparative study of atomic fluorescence spectroscopy and inductively coupled plasma mass spectrometry for mercury and arsenic multispeciation. Anal Bioanal Chem 2005;382:485–92.
[18] Chen S, Wang X, Niu Y, et al. Simple and cost-effective methods for precise analysis of trace element abundances in geological materials with ICP-MS. Sci Bull 2017;62:277–89.
[19] Meng W, Liu P, Cai P, et al. An ultrasensitive method for detecting picomolar levels of cadmium (II) by fast-scan anodic stripping voltammetry. Int J Electrochem Sci 2018;13:11808–18.
[20] Chen X, Hong F, Zhang W, et al. Microchip electrophoresis based multiplexed assay for silver and mercury ions simultaneous detection in complex samples using a stirring bar modified with encoded hairpin probes for specific extraction. J Chromatogr A 2019;1589:173–81.
[21] Liu X, Tang Y, Wang L, et al. Optical detection of mercury (II) in aqueous solutions by using conjugated polymers and label-free oligonucleotides. Adv Mater 2007;19:1471–4.
[22] He S, Song B, Li D, et al. A graphene nanoprobe for rapid, sensitive, and multicolor fluorescent DNA analysis. Adv Funct Mater 2010;20:453–9.
[23] Wen Y, Xing F, He S, et al. A graphene-based fluorescent nanoprobe for silver (I) ions detection by using graphene oxide and a silver-specific oligonucleotide. Chem Commun 2010;46:2596–8.
[24] Srinivasan K, Subramanian K, Rajasekar A, et al. A sensitive optical sensor based on DNA-labelled Si@SiO_2 core-shell nanoparticle for the detection of Hg^{2+} ions in environmental water samples. Bull Mat Sci 2017;40:1455–62.
[25] Chu J, Park C, Jang K, et al. A technique for highly sensitive detection of mercury ions using DNA-functionalized gold nanoparticles and resonators based on a resonance frequency shift. J Mech Sci Technol 2018;32:799–804.
[26] Zhang L, Li T, Li B, et al. Carbon nanotube-DNA hybrid fluorescent sensor for sensitive and selective detection of mercury (II) ion. Chem Commun 2010;46:1476–8.
[27] Song T, Zhu X, Zhou S, et al. DNA derived fluorescent bio-dots for sensitive detection of mercury and silver ions in aqueous solution. Appl Surf Sci 2015;347:505–13.
[28] Du J, Jiang L, Shao Q, et al. Colorimetric detection of mercury ions based on plasmonic nanoparticles. Small 2013;9:1467–81.
[29] Deng L, Zhou Z, Li J, et al. Fluorescent silver nanoclusters in hybridized DNA duplexes for the turn-on detection of Hg^{2+} ions. Chem Commun 2011;47:11065–7.
[30] He D, He X, Wang K, et al. Intracellular acid-triggered drug delivery system using mesoporous silica nanoparticles capped with T-Hg^{2+}-T base pairs mediated duplex DNA. J Mater Chem B 2013;1:1552–60.
[31] Wu LL, Wang Z, Zhao SN, et al. A metal-organic framework/DNA hybrid system as a novel fluorescent biosensor for mercury (II) ion detection. Chem Eur J 2016;22:477–80.
[32] Smith SB, Cui Y, Bustamante C. Overstretching B-DNA: the elastic response of individual double-stranded and single-stranded DNA molecules. Science 1996;271:795–9.
[33] Lin N, Dufresne A. Physical and/or chemical compatibilization of extruded cellulose nanocrystal reinforced polystyrene nanocomposites. Macromolecules 2013;46:5570–83.
[34] Sacui IA, Nieuwendaal RC, Burnett DJ, et al. Comparison of the properties of cellulose nanocrystals and cellulose nanofibrils isolated from bacteria, tunicate, and wood processed using acid, enzymatic, mechanical, and oxidative methods. ACS Appl Mater Interfaces 2014;6:6127–38.
[35] Lin N, Bruzzese C, Dufresne A. TEMPO-oxidized nanocellulose participating as crosslinking aid for alginate-based sponges. ACS Appl Mater Inter 2012;4:4948–59.
[36] Montanari S, Roumani M, Heux L, et al. Topochemistry of carboxylated cellulose nanocrystals resulting from TEMPO-mediated oxidation. Macromolecules 2005;38:1665–71.
[37] Jiang J, Ye W, Liu L, et al. Cellulose nanofibers prepared using the TEMPO/Laccase/O_2 system. Biomacromolecules 2016;18:288–94.
[38] Araki J, Wada M, Kuga S. Steric stabilization of a cellulose microcrystal suspension by poly (ethylene glycol) grafting. Langmuir 2001;17:21–7.
[39] Majoinen J, Walther A, McKee JR, et al. Polyelectrolyte brushes grafted from cellulose nanocrystals using Cu-mediated surface-initiated controlled radical polymerization. Biomacromolecules 2011;12:2997–3006.
[40] Habibi Y, Chanzy H, Vignon MR. TEMPO-mediated surface oxidation of cellulose whiskers. Cellulose 2006;13:679–87.
[41] Kiy MM, Jacobi ZE, Liu J. Metal-induced specific and nonspecific oligonucleotide folding studied by FRET and related biophysical and bioanalytical implications. Chem Eur J 2012;18:1202–8.
[42] Follain N, Marais MF, Montanari S, et al. Coupling onto surface carboxylated cellulose nanocrystals. Polymer 2010;51:5332–44.
[43] Mangalam AP, Simonsen J, Benight AS. Cellulose/DNA hybrid nanomaterials. Biomacromolecules 2009;10:497–504.

Lin Gan got his Ph.D. degree in Sun Yat-sen University and focused on polymer chemistry and physics. Now he is engaged in biomass polymers and nanomaterials with photonic and electric functions.

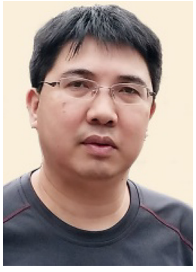

Jin Huang got his Ph.D. degree in Wuhan University. Now he is engaged in natural polymers chemistry, bio-based materials and composites based on natural polymer chemistry and soft-matter nanotechnology.